

Detections of Molecular Hydrogen in the Outer Filaments of NGC 1275

N. A. Hatch,* C. S. Crawford, A. C. Fabian and R. M. Johnstone

Institute of Astronomy, Madingley Road, Cambridge, CB3 0HA

11 October 2018

ABSTRACT

We present clear spectroscopic detections of molecular hydrogen in the outer filaments of the H α nebula surrounding the central galaxy of the Perseus cluster, NGC 1275. This implies the presence of warm molecular gas clouds at projected distances up to 24 kpc from the nucleus of the host galaxy, embedded in the hot intracluster medium. The emission-line intensity ratios reveal that the H₂ emission is predominately thermally excited with excitation temperatures of 1600–2200 K, suggesting a lack of pressure balance between the molecular component and its surrounding medium. Excitation by stellar UV or by the central AGN is shown to be unlikely, whilst thermal excitation by X-rays or conduction from the ICM or shocks are all possibilities. Evidence for a non-thermal component is found in the spectra of some regions based on a low ortho-to-para ratio.

Key words: galaxies: clusters: individual: Perseus - cooling flows - galaxies: individual: NGC 1275 - intergalactic medium - infrared: galaxies.

1 INTRODUCTION

Luminous optical and UV line-emitting filamentary nebulae like that of NGC 1275 are commonly found surrounding central cluster galaxies where the X-ray emitting intracluster medium (ICM) has a short radiative cooling time (Crawford et al. 1999 and references therein). Despite many studies, the origin and excitation mechanism of these filaments are uncertain, with cooling of the intracluster gas, star formation, conduction and shock heating all having been suggested and contested (e.g. Johnstone & Fabian 1988, Sabra et al. 2000).

The large H α nebulosity surrounding NGC 1275 has been long known (Minkowski 1957, Lynds 1970) and has been studied in a variety of wavelengths. Deep H α and X-ray images obtained by the WIYN telescope (Conselice et al. 2001) and Chandra (Fabian et al. 2003) show spectacular, extended H α filamentary structures stretching over 50 kpc from the central galaxy, with corresponding soft X-ray counterparts, deeply embedded in the hot ICM.

NGC 1275 lies at the centre of a cluster with strong centrally peaked X-ray emission where the X-ray luminosity implies a mass deposition rate of $300 M_{\odot} \text{yr}^{-1}$ (Allen et al. 2001). However, after extensive searching, the massive amounts of gas expected to accumulate cannot be accounted for as stars or line-emitting gas near the nucleus.

Chandra spectra show little evidence of gas cooling below a temperature about one third of that in the bulk of the cluster (Schmidt et al. 2002; Sanders et al. 2004). Therefore most of the

gas either cools further in a non-radiative manner, requiring energy to be shared between the hot X-ray emitting and cooler gas by mixing or conduction, or is heated by a distributed heat source. A number of theories including heating by the central active galactic nucleus (AGN) of NGC 1275 have been suggested (see Fabian 2004 and references therein).

A reservoir of $\sim 4 \times 10^6 M_{\odot}$ (Heckman et al. 1989) of $10^4 - 10^5$ K gas lies in the optical and UV line-emitting nebula. Molecular gas appears common in such regions (Jaffe & Bremer 1997). Recent observations show that there is a component of warm (1000–4000 K) molecular hydrogen gas (Donahue et al. 2000; Edge et al. 2002) with up to $\sim 1 \times 10^{10} M_{\odot}$ of cool molecular gas (Edge 2001). Krabbe et al. (2000) and Donahue et al. (2000) deduced that the molecular hydrogen component in the NGC 1275 nuclear region is likely to be excited by the central AGN, whilst Wilman et al. (2002) argue that the H₂ emission is thermal and mostly likely to be heated by UV radiation. The outer filaments have a fairly constant H α surface brightness extending over many tens of kpc, therefore a central excitation source such as the AGN is unlikely to be of great importance. Whilst massive stellar clusters are seen in H α , they do not spatially correspond with all the filaments and bright knots. Thus the excitation of the outer filaments may be different to that of the nuclear region.

The redshift of NGC 1275 is 0.0176, which using $H_0 = 70 \text{ km s}^{-1} \text{ Mpc}^{-1}$, gives $1 \text{ kpc} \simeq 2.7 \text{ arcsec}$.

* E-mail: nah@ast.cam.ac.uk

Target	Slit centre co-ordinates		Position angle	Nodding (arcsec)	Total integration time on target (minutes)
	RA	Dec (J2000)			
Slit 1 (NW)	03 19 46.78	+41 31 45.28	-125°	0, -10	36
Slit 2 (SW)	03 19 41.95	+41 29 58.61	-76°	-30, -20	48
Slit 3 (E)	03 19 49.31	+41 31 50.52	-4°	-35, -80	54

Table 1. Log of Observations. Nodding \pm direction and position angle as explained in CGS4 literature.

2 OBSERVATIONS

The spectra presented in this paper were taken with the CGS4 spectrograph on the United Kingdom Infrared Telescope on 2004 January 17, 18 and 19 for a total integration time of 15 hours. The 40 lines mm^{-1} grating was used with the 300 mm focal length camera, giving a spatial scale of 0.61 arcsec per pixel. The B2 filter centred at 2.02 μm was used with a two pixel wide slit giving a spectral resolution of 600–790 kms^{-1} . The observations were taken in ND-STARE mode, using a object-sky-sky-object nodding pattern. The seeing was better than one arcsec on all three nights and there was little to no cloud cover.

The telescope was directed to a bright reference source near the target position. The slit was then shifted to a targeted bright object (co-ordinates given in Table 1) and orientated to the correct position angle. For confirmation of the exact spatial position of the slit we included one or two bright objects such as a star or galaxy along the length of the slit. Table 1 gives the co-ordinates, position angle and integration time for all observations. Guided by the H α map of Conselice et al. (2001), the slit positions were chosen to include some of the brightest knots and filaments furthest from the nucleus.

Most sky emission features were removed automatically by the nodding pattern. An atmospheric, temporally variable CO₂ line near 2.01 μm and a feature at 2.15 μm however remain in the spectrum from the Slit 1 and 2 position. The target observations were preceded and followed by a series of calibration observations including flat-fields, dark frames, arcs and a set of standard F and G type stars. These standards were nearly featureless stars of known magnitude. In each of the standard stars a Bry stellar feature at 2.166 μm was removed by linear interpolation. The data was reduced with ORAC-DR Version V4.0-1 available through the UKIRT software website. Data manipulation and extraction was done with Starlink packages, QDP (Tennant 1990) and IDL Version 6.0.

3 RESULTS

Clear detections of the strongest molecular hydrogen lines: $v=1-0$ S(1) and $v=1-0$ S(3) were found in seven separate regions of the outer filaments, marked and labelled in Fig. 1. Region A covers an area of very strong H α emission. Shields & Filippenko (1990) discovered and studied a massive, young stellar cluster in this region. It lies 19.4 arcsec (a projected distance of 7.2 kpc) to the East of the central galaxy, marked as a bright knot in H α within the Northern bright filament that is part of array of radial filaments that point East from the galaxy. Regions B, C and D come from this array of radial filaments at distances 18.0 arcsec (6.7 kpc), 17.7 arcsec (6.6 kpc), 17.9 arcsec (6.6 kpc) from the central galaxy respectively. There is no clear distinction separating regions C and D in the slit image, although spectral analysis revealed they were most likely separate populations of molecular hydrogen. The ‘horseshoe knot’

Region	Line	Surface Brightness
RA	Dec (J2000)	
size of extracted region		
Horseshoe knot	$v=1-0$ S(3)	20.7 $^{+3.6}_{-3.3}$
03 19 45.22	+41 31 32.61	6.6 $^{+2.8}_{-2.5}$
2.23 arcsec ²	$v=1-0$ S(1)	18.1 $^{+3.2}_{-2.8}$
	$v=1-0$ S(0)	5.2 $^{+3.6}_{-2.1}$
SW1 knot	P α	11.5 $^{+7.2}_{-4.1}$
03 19 45.69	+41 29 46.99	7.5 $^{+2.9}_{-2.7}$
4.47 arcsec ²	$v=1-0$ S(3)	13.1 $^{+1.8}_{-1.7}$
	$v=1-0$ S(2)	2.6 ± 1.4
	$v=1-0$ S(1)	15.3 $^{+2.3}_{-2.1}$
	$v=1-0$ S(0)	4.9 $^{+1.9}_{-1.8}$
	$v=1-0$ Q(1)	14.7 $^{+4.3}_{-4.2}$
SW2 knot	$v=1-0$ S(3)	4.6 $^{+2.7}_{-2.2}$
03 19 44.97	+41 29 48.92	5.6 $^{+2.1}_{-1.9}$
2.98 arcsec ²	$v=1-0$ S(1)	
Region A	P α (Narrow)	119.1 ± 35.6
03 19 49.71	+41 30 51.11	38.7 ± 35.6
2.23 arcsec ²	P α (Broad)	
	$v=1-0$ S(3)	4.6 $^{+1.3}_{-1.4}$
	$v=1-0$ S(1)	6.5 $^{+1.7}_{-1.9}$
	Bry	8.3 $^{+5.6}_{-2.6}$
Region B	P α	45.1 $^{+10.9}_{-9.0}$
03 19 49.75	+41 30 45.19	23.5 $^{+2.6}_{-2.5}$
2.23 arcsec ²	$v=1-0$ S(3)	12.5 $^{+2.6}_{-2.4}$
	$v=1-0$ S(2)	24.5 $^{+2.5}_{-2.3}$
	$v=1-0$ S(1)	9.8 $^{+2.7}_{-2.4}$
	$v=1-0$ S(0)	17.2 $^{+5.3}_{-4.9}$
	$v=1-0$ Q(1)	18.6 $^{+8.5}_{-6.5}$
Region C	P α	25.5 $^{+6.4}_{-6.1}$
03 19 49.77	+41 30 43.24	16.8 ± 1.9
2.98 arcsec ²	$v=1-0$ S(3)	7.3 $^{+1.9}_{-1.7}$
	$v=1-0$ S(2)	10.5 ± 1.6
	$v=1-0$ S(1)	4.6 $^{+1.7}_{-1.6}$
	$v=1-0$ S(0)	10.2 $^{+4.4}_{-4.2}$
Region D	$v=1-0$ S(3)	10.3 $^{+3.0}_{-2.5}$
03 19 49.77	+41 30 41.28	5.1 $^{+1.5}_{-0.4}$
2.23 arcsec ²	$v=1-0$ S(1)	

Table 2. Line surface brightness in $10^{-17}\text{erg s}^{-1}\text{cm}^{-2}\text{arcsec}^{-2}$ for all regions (as marked in Fig. 1) in which the strongest ro-vibrational H₂ lines, $v=1-0$ S(1) and $v=1-0$ S(3) are clearly detected. Errors are at 1 σ level.

lies at the tip of a horseshoe-shaped feature at the end of a 74 arcsec long NW radial filament that appears to turn back on itself, noted by Conselice et al. (2001) (box 11 in their Fig. 5). It has a projected distance of 22 kpc away from the galaxy center. SW1 (box 2 in Conselice et al. 2001 Fig. 5) and SW2 are bright knots that lie at the end of radial filaments (61.6 arcsec \sim 23 kpc and 64.6 arcsec \sim 24 kpc from the galaxy respectively) pointing SSW. Our K-band

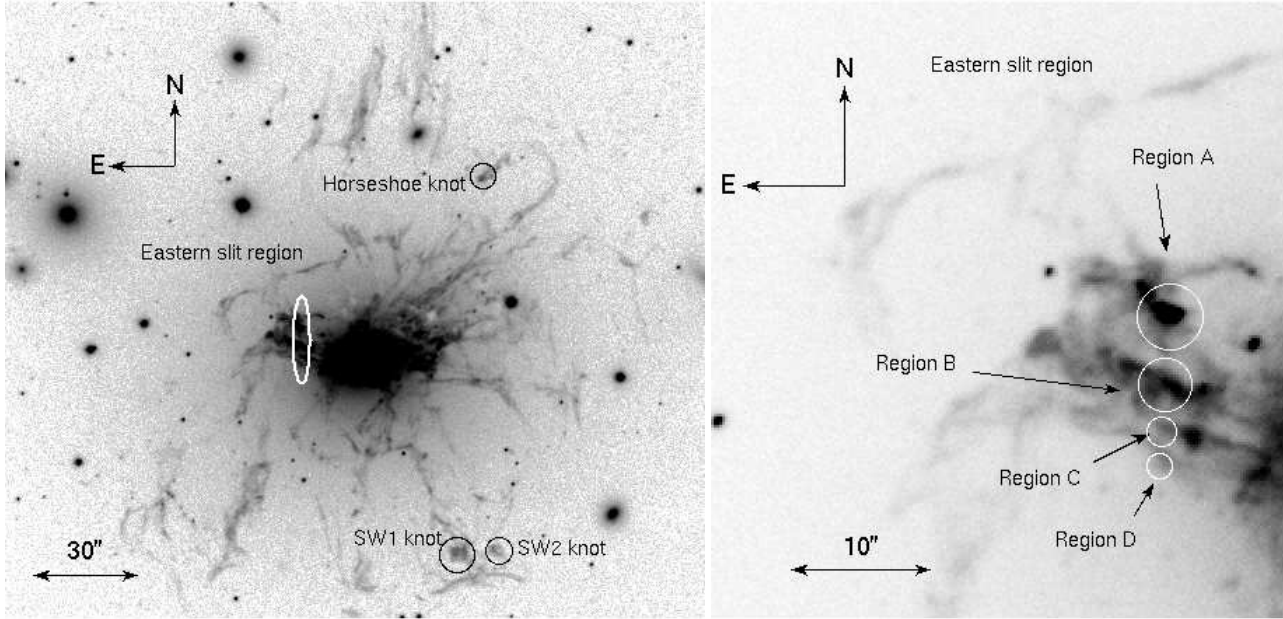


Figure 1. Left: WIYN telescope H α image of the line-emitting filamentary structure surrounding NGC1275 from Conselice et al. (2001). Regions where H $_2$ ro-vibrational lines are detected have been marked by circles and labelled. Right: Detail of the Eastern slit region.

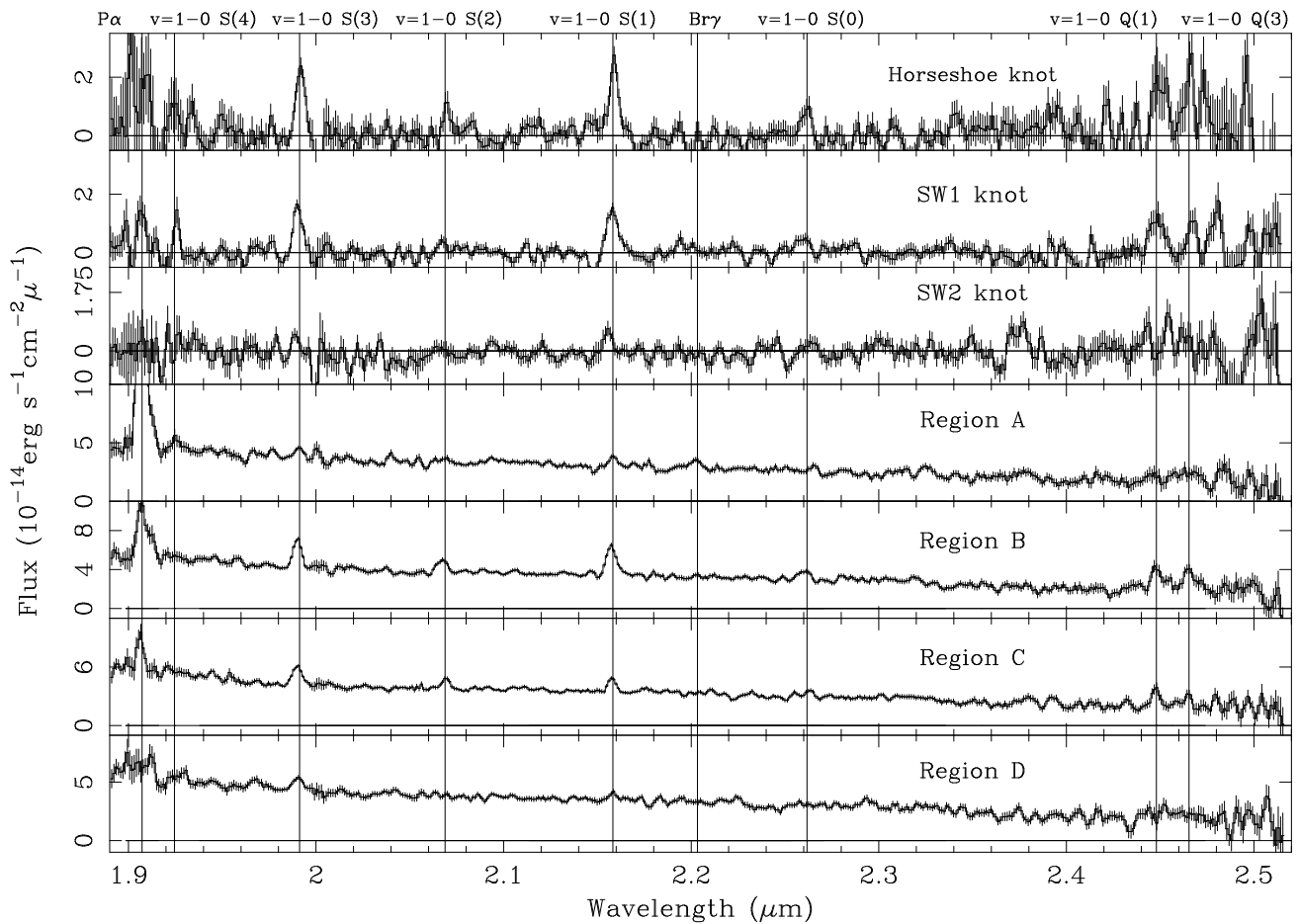


Figure 2. UKIRT K-band smoothed spectra of the outer filament regions marked in Fig. 1 with the ro-vibrational H $_2$ and atomic hydrogen lines labelled. Line labels have redshift $z=0.0172$. Errors are from Poisson Statistics. Note that the scale in Region A does not show full extent of P α .

spectra for all regions are presented in Fig. 2, with line surface brightness given in Table 2. Since the structures observed may be smaller than the slit size, these intensities may be underestimated, hence they could be considered lower limits. The spectra have not had any stellar continuum removed. The SW regions and the horseshoe knot show no evidence for a continuum, whereas regions A, B, C and D all have a continuum due to the galactic stellar emission.

In principle the wavelength range should allow an estimation of the extinction using the $P\alpha$ and $B\gamma$ lines or from the $v=1-0$ Q(3) and $v=1-0$ S(1) lines. However the $P\alpha$ and $v=1-0$ Q(3) emission lines pass through complex parts of the atmospheric window and the $B\gamma$ emission is too faint to have a significant detection in all but one region. Therefore no reddening has been taken into account in this work, although we note any consequence it may have in our discussion of the data.

4 ANALYSIS AND DISCUSSION

4.1 Velocity Structure

The $P\alpha$ emission from regions A and B both exhibit non-Gaussian profiles, shown in Fig. 3. This profile could not occur through line blending as the $P\alpha$ line is distinct from the other molecular and atomic hydrogen lines. These profiles may be the result of either extra redshifted material or absorption of the blueshifted emission, either intrinsically or by the Earth's atmosphere (this line is located in a complex part of the atmospheric window). Neither the molecular hydrogen lines nor the other atomic lines from our spectra exhibit these profiles, although given the high $P\alpha/H_2$ line ratio of region A, it is unlikely that a low flux red wing would be visible in the molecular emission above the noise level.

The $H\alpha$ emission from region A has been studied by Shields et al. (1990) who find the $H\alpha$ profile shows a well defined narrow peak at $z=0.0168$ and a large bump of emission at a larger redshift. They interpret the lower redshift, narrow emission as originating from the stellar cluster, and the broad emission originating from overlapping filamentary material. From the $[O I]/H\alpha$ ratio they estimated approximately 30 per cent of the total $H\alpha$ luminosity in this region originates from the filament. The $P\alpha$ emission profile from region A can be better fitted by two Gaussians, a narrow Gaussian at $z\sim 0.0165$ containing 75 per cent of the total line emission and a broad Gaussian containing 25 per cent of the line emission with $z\sim 0.018$, rather than a single Gaussian. Although our slit may not have covered the exact same region investigated by Shields et al. (1990), the similarities in line profile suggest the same interpretation.

Region B can also be fitted by two Gaussians; a broad dominating component at $z\sim 0.0169$ and a narrow component at a much larger redshift. The large errors and lack of other corroborating evidence makes it difficult to apply an intrinsic emission interpretation to this region as opposed to absorption by the atmosphere. Therefore a single Gaussian profile is fitted to the $P\alpha$ emission.

None of the lines were resolved spectrally but Fig. 4 shows that there is a velocity shift relative to the nucleus of the strong H_2 lines: $v=1-0$ S(1), $v=1-0$ S(2), $v=1-0$ S(3) and $P\alpha$ emission. This figure shows the molecular and atomic emission from regions B, C and the SW1 knot appear to have similar velocity shifts, therefore it is likely they share an origin. The $B\gamma$ emission from region A has a similar velocity shift to the narrow $P\alpha$ emission, therefore most likely to have originated from the same region, the stellar cluster. The molecular emission from region A does not share the same

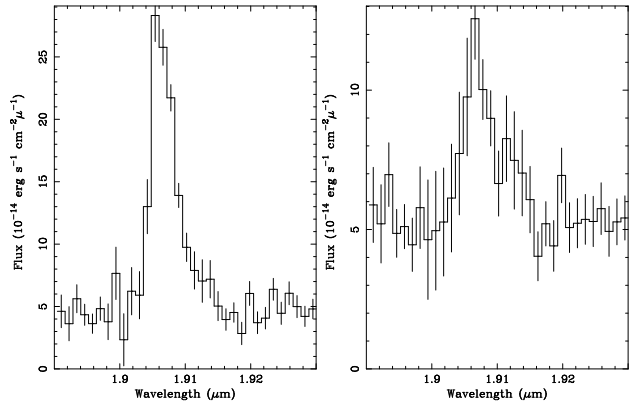


Figure 3. $P\alpha$ line emission from region A, the young stellar cluster (left) and region B (right), both showing non-Gaussian profiles.

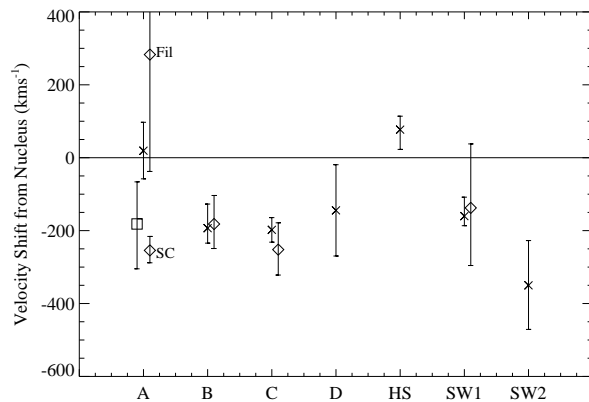


Figure 4. Velocity shift of molecular and atomic hydrogen lines relative to the nucleus, measured from a combined fit of the $v=1-0$ S(1), $v=1-0$ S(2) and $v=1-0$ S(3) lines (crosses), $P\alpha$ lines (diamonds), $B\gamma$ (square). HS is the horseshoe knot. The velocity shift of both the narrow $P\alpha$ emission labelled A(SC) and the broad emission labelled A(fil) are shown. Velocity resolution is approximately 700 km s^{-1} , errors reflect 1σ level on line position. Nuclear molecular hydrogen line positions from Krabbe et al. (2000); nuclear $P\alpha$ ($1.8756 \mu\text{m}$) and $B\gamma$ ($2.1661 \mu\text{m}$) line positions chosen to conform with redshift of $z=0.0172$ as measured by Krabbe et al. (2000)

velocity shift as either the stellar cluster or the filament. It is possible the molecular hydrogen emission is a superposition of emission from both the filament and the stellar cluster, or the molecular emission may not share the same origin as the atomic emission. If the $P\alpha$ emission was fit with a single profile, the velocity shifts of the $P\alpha$ and the H_2 would still not agree. This figure suggests that the outer filaments observed are systematically blueshifted relative to the nucleus.

4.2 H_2 Excitation

H_2 excitation may occur through collisions and therefore exhibit thermal emission, or from radiative transfers producing non-thermal emission. These mechanisms can be distinguished since they preferentially populate different levels producing different spectra, but as they often occur together the observed spectra can exhibit both thermal and non-thermal emission. Collisional de-excitation dominates when the gas has a total den-

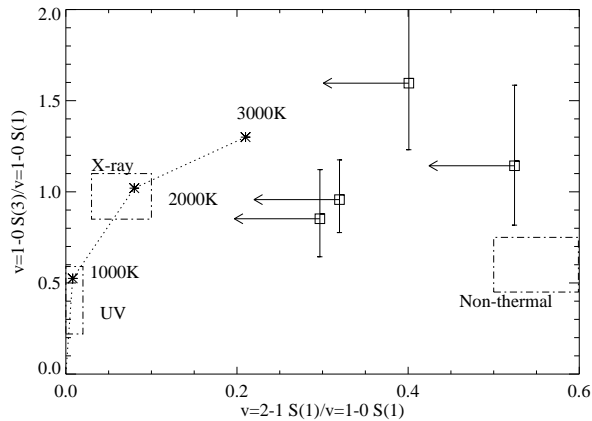


Figure 5. Diagram constraining likely excitation mechanisms. The four 3σ upper limits indicate observed line ratios from the brightest filaments, errors on the $v=1-0$ S(1)/ $v=1-0$ S(3) ratio are 1σ level. Boxes highlight regions occupied by the non-thermal UV excitation models of Black & van Dishoeck (1987) and models of thermal processes near the dotted thermal curve including UV excitation (Sternberg & Dalgarno 1989) and X-ray heating models (Lepp & McCray 1983 and Draine & Woods 1990). The x-axis gives an indication of the level of thermal to non-thermal excitation occurring. The upper limits are consistent with a thermal excitation mechanism, but there also may be a non-thermal component.

sity $n_T = n_{\text{H}} + n_{\text{H}_2} \geq 10^4 \text{ cm}^{-3}$ (Sternberg & Dalgarno 1989; Mandy & Martin 1993) for $T \sim 10^3$ K. The gas may be heated by shocks, conduction from the ICM, X-rays or UV photons and the H_2 energy levels populated through collisional transitions. When this occurs the ortho-to-para ratio is three and the gas is in local thermodynamic equilibrium (LTE). Below the critical density, the probability of the H_2 undergoing a transition from an upper to a lower energy level via a radiative process is greater than for collisional de-excitation. The H_2 molecules can be excited to the upper energy levels through non-thermal excitation mechanisms such as X-rays and UV photons in the Lyman-Werner band (912–1108Å) or through collisions with suprathermal electrons caused by X-ray ionization.

Non-thermal excitation mechanisms readily excites the $v = 2$ and higher vibrational states, whereby collisional transitions preferentially de-excite the $v = 2$ level in favour of the $v = 1$ level, so the $v=2-1$ S(1)/ $v=1-0$ S(1) ratio is an indicator of the relative level of thermal to non-thermal processes. Reddening does not have a large effect in this part of the spectrum, therefore it can be ignored without much consequence when considering H_2 line ratios. Models predict a $v=2-1$ S(1)/ $v=1-0$ S(1) ratio greater than 0.53 for pure fluorescence at $n_T \leq 10^5 \text{ cm}^{-3}$ and low temperatures (Draine & Bertoldi 1996), whilst shock models of Hollenbach & McKee (1989) exhibit ratios between 0.04–0.46. 3σ upper limits of the $v=2-1$ S(1) emission from the four regions exhibiting the strongest H_2 lines and best signal-to-noise ratio (region A, region B, SW2, horseshoe knot) are plotted in an excitation diagram (Fig. 5). All lines used in these ratios are ortho, so this diagram is independent of an uncertain ortho-to-para ratio. Fig. 5 is consistent with predominately thermal (collisional) excitation occurring but does not rule out a non-thermal component.

If collisional de-excitation is assumed to dominate, the H_2 will be in local thermal equilibrium (LTE). The energy levels of H_2 will be populated in a Boltzmann distribution and from this an excita-

tion temperature (T_{ex}) can be derived through

$$\frac{N(v, J)}{gJ} = a e^{-E(v, J)/k_{\text{B}}T_{\text{ex}}}$$

where $E(v, J)$ is the upper energy of the (v, J) transition, a is a constant, k_{B} is Boltzmann's constant and g_J is the statistical weight. $N(v, J)$ is the transition column density, which, for optically-thin emission is given by

$$N(v, J) = \frac{4\pi I}{A_{\text{ul}} h \nu}$$

where I is the observed intensity of the line, ν is the rest frequency and A_{ul} is the Einstein co-efficient taken from Turner et al. (1977). In all calculations an ortho-to-para ratio of 3:1 has been assumed. If the H_2 is only thermally excited, the excitation temperature is the kinetic temperature. However, if non-thermal excitation is also taking place, the excitation temperature is not the actual temperature of the gas, but characterises the level populations that have arisen through competing thermal and non-thermal processes (Puxley et al. 2000).

The LTE plots (Fig. 6) show the horseshoe knot spectrum fits a model of thermalised gas with an ortho-to-para ratio of three. The LTE plots of regions B and C show a clear misalignment of the ortho (odd J) and para (even J) lines which indicate a lower ortho-to-para ratio. The $v=1-0$ S(4) line (and possibly $v=1-0$ S(2)) are much narrower than the other molecular lines from the SW1 region, possibly affected by atmospheric sky subtraction (see Fig. 2). The S(0) line appears to agree with a model of thermalised gas with an ortho-to-para ratio of three, whilst the S(2) and S(4) lines do not.

Molecular hydrogen is formed with an ortho-to-para ratio of three. No radiative process can induce conversions between the ortho and para lines, hence the ratio is conserved. There are three known methods in which ortho-to-para conversions can occur: by collisions with protons in cold ($T < 100\text{K}$) gas, or collisions with hydrogen atoms in warmer gas ($T < 300\text{K}$). Finally, if the hydrogen molecule stays on a grain long enough it can evaporate with an ortho-to-para ratio appropriate to the grain temperature. In regions where shock excitation is the primary excitation mechanism, the rapid collisions cause the ortho-to-para ratio to take on a value close to three (Smith et al. 1997). However photodissociation regions (PDRs) often exhibit lower ortho-to-para ratios, typically 1.5–2.2. Sternberg & Neufeld (1999) provides models of far-UV (FUV) pumping in PDRs with optically thick H_2 ($\sim 10^{14} \text{ cm}^{-2}$ for UV) which explain how the observed ortho-to-para ratio will tend to 1.7 whilst the true ortho-to-para ratio remains at three due to lower rates of FUV pumping of molecular hydrogen in the optically thicker ortho states compared to the para states. In these models, the gas density must remain below $5 \times 10^4 \text{ cm}^{-3}$ and be relatively cool ($T < 1000\text{K}$) in order for collisional excitation to be negligible relative to FUV pumping, and collisional de-excitation to be negligible compared to spontaneous radiative decay, otherwise the ortho-to-para ratio would tend to the LTE value of three.

We follow Draine & Bertoldi (1996) definition of the ortho-to-para ratio, γ

$$\gamma = \frac{3a_{\text{ortho}}}{a_{\text{para}}}$$

This ratio can be determined from a single pair of one ortho and one para line (Puxley et al. 2000) through

$$\gamma = \frac{I_o A_p (2J_p + 1) \lambda_o}{I_p A_o (2J_o + 1) \lambda_p} e^{\Delta E_{po}/k_{\text{B}}T_{\text{ex}}}$$

where λ is the wavelength, J is the rotational quantum number

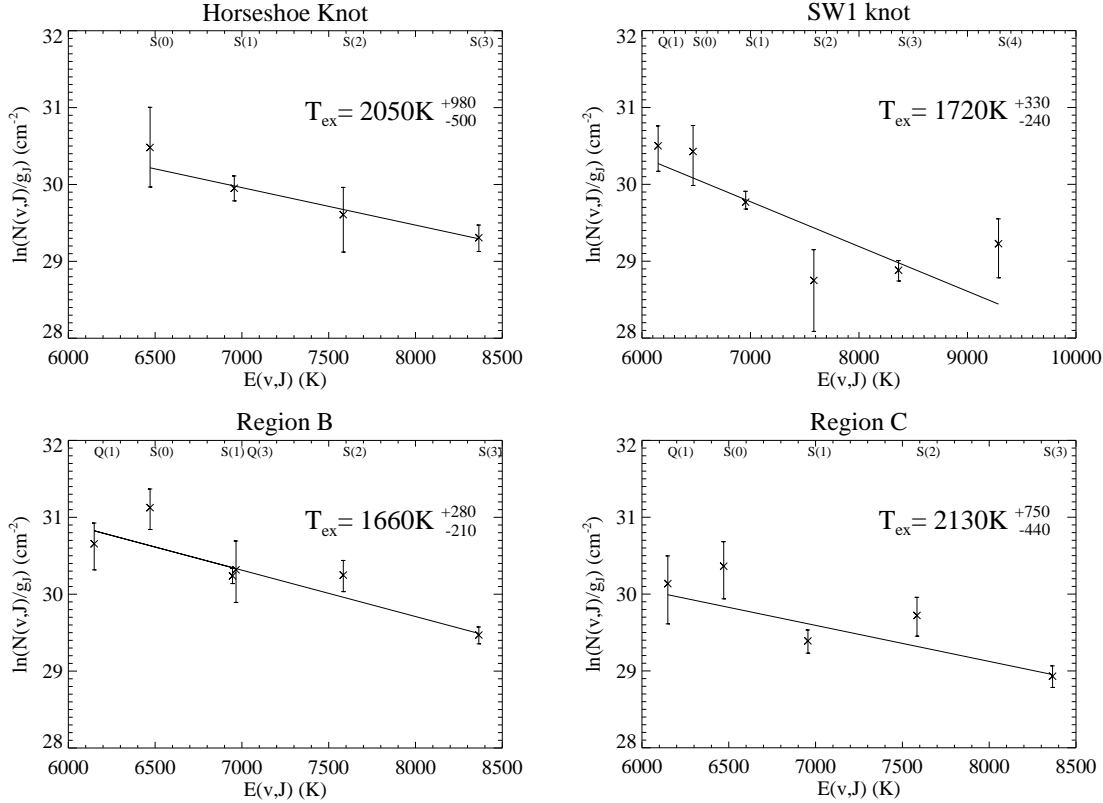


Figure 6. Local thermodynamic equilibrium plots, where the inverse slope of the best fit line gives T_{ex} . Errors on data points are at 1σ level, and error on T_{ex} is 1σ error from weighted best fit. The labels refer to the $v=1-0$ S and Q transitions. $v=1-0$ S(1) and $v=1-0$ Q(3) transitions have been offset in region B for clarity.

of the upper state of the transition and ΔE_{po} is the energy difference between the upper energy level of the para and ortho line. Ortho/para lines are denoted by a o/p subscript.

T_{ex} and ortho-to para ratios are given in Table 3 for regions B, C, SW1, and the horseshoe knot, where three or more H₂ lines are detected. The excitation temperature of the molecular hydrogen gas in the centre of NGC 1275 is given by Wilman et al. (2002) to be 1620 K, whereas Krabbe et al. (2000) measure it to be 1450 ± 250 K (from the $v=1$ transitions). T_{ex} of the filaments are consistent with these values for the gas in the core of the nebula, although tend to be slightly higher.

Although there are large errors, the ortho-to-para ratios suggests that regions B and C may also be non-thermally excited, possibly by FUV pumping in a PDR.

Assuming the upper levels are also populated in a Boltzmann distribution at the same excitation temperature, the total H₂ column density is given by

$$N_{\text{Total}} = \frac{N(v,J)Z(T)}{g_l e^{-E(v,J)/k_b T_{\text{ex}}}}$$

where $Z(T)$ is the partition function. This expression assumes all the molecular hydrogen is collisionally excited at the same temperature and all the emission is visible. There are many scenarios in which this may not be the case, such as the X-ray dissociated regions modelled by Maloney et al. (1996). In addition the line surface brightness listed in Table 2 are only lower limits, therefore these column densities can be considered lower limits also.

Column densities are listed for each region with three or more strong H₂ lines in Table 3. If T_{ex} of the upper levels is greater than

in the lower levels, the column density will decrease from these values. All column densities are low ($2-14 \times 10^{15} \text{cm}^{-2}$) which has implications for the structure of the filaments. For the gas to be thermalised the total density must be greater than 10^4cm^{-3} . The H α filaments are estimated to have a density of $\sim 10^2 \text{cm}^{-3}$ assuming they are in pressure equilibrium with the surrounding X-ray emitting gas. The filaments must thus have an undetected denser and cooler (1600-2200 K) atomic component that mixes and shares energy with the molecular hydrogen. Alternatively, the H₂ exists in clumps, much smaller than a parsec in diameter, strung through the H α filaments. This has parallels with suggestions of Fabian et al. (2003) that the atomic hydrogen has a similar structure, on the basis of the H α emission and pressure balance. Consistently Wilman et al. (2002) argue that the H₂ emission near the nucleus of NGC 1275 must come from a population of dense self-gravitating clouds based on H₂ line ratios.

4.3 Comparison of Molecular and Atomic Hydrogen Emission

Comparing our results with the H α distribution of Conselice et al. (2001) (reproduced partly here in Fig. 1), we find the molecular hydrogen emission is clearly associated with the atomic emission, suggesting a common excitation mechanism.

Molecular to atomic line ratios are commonly used to distinguish between various excitation mechanisms. 3σ upper limits of Br γ were taken from our spectra and estimates of the H α emission

Region	Excitation Temperature (K)	ortho-to-para ratio (γ)	H ₂ Column Density (10^{15} cm^{-2})
Horseshoe knot	$2050 \pm_{500}^{980}$	$2.8 \pm_{1.3}^{2.5}$	7.7 ± 2.0
SW1 knot	$1720 \pm_{240}^{330}$	$3.0 \pm_{1.2}^{3.2}$	10.1 ± 1.6
Region B	$1660 \pm_{210}^{280}$	$1.9 \pm_{0.5}^{0.8}$	13.5 ± 3.1
Region C	$2130 \pm_{440}^{750}$	$1.7 \pm_{0.6}^{1.0}$	2.5 ± 1.0

Table 3. Excitation temperature, ortho-to-para ratios and total line-emitting molecular hydrogen column density of all regions observed which revealed more than two molecular hydrogen lines. Errors correspond to the 1σ level.

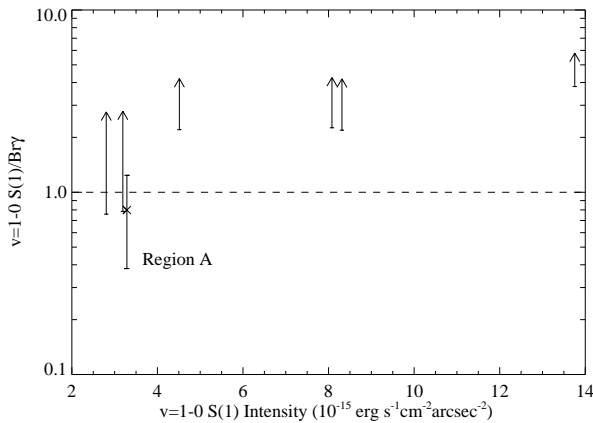


Figure 7. The line intensity ratio $v=1-0 \text{ S}(1)/\text{Br}\gamma$ plotted against $v=1-0 \text{ S}(1)$ intensity. $v=1-0 \text{ S}(1)$ line has 1σ errors, whilst $\text{Br}\gamma$ line is a 3σ upper limit. Region A is labelled. Active galaxies and starforming regions have a ratio ≤ 1 (below the dashed line). The weakness of the $\text{Br}\gamma$ line rules out stellar UV as a possible excitation mechanism

from Fig. 5 of Conselice et al. (2001) are used in conjunction with the strong $v=1-0 \text{ S}(1)$ line to constrain excitation models.

Active galaxies (starburst, Seyfert and ultra luminous IR galaxies) and star forming regions have the ratio $v=1-0 \text{ S}(1)/\text{Br}\gamma \leq 1$ (Jaffe et al. 2001) whereas most of the filament regions observed here have $v=1-0 \text{ S}(1)/\text{Br}\gamma \geq 1$ (Fig. 7), which strongly argues against a stellar UV excitation model. The exception is region A, which has a spectrum with $v=1-0 \text{ S}(1)/\text{Br}\gamma \leq 1$, although the molecular and $\text{Br}\gamma$ emission may have different origins as Fig.4 suggests. All regions observed, except region A, do not show evidence for stars in the continuum images (Conselice et al. 2001) and regions further from the galaxy (SW1, SW2 and the horseshoe knot) do not show a continuum in their K-band spectra (Fig. 2). It therefore seems unlikely that these regions can be excited by UV photons from young, hot stellar populations. However $\text{Ly}\alpha$ emission and UV continuum has been found associated with the optical filaments (Fabian et al. 1984; Norgaard-Nielsen et al. 1990) that may not have originated from stars.

The $v=1-0 \text{ S}(1)/\text{H}\alpha$ ratios for the outer filaments, shown in Fig. 8, generally lie between 0.02-0.1, similar to ratios from the centre of other dominant cluster galaxies. In the central region of NGC 1275 Donahue et al. (2000) show the $v=1-0 \text{ S}(1)/\text{H}\alpha$ ratio decrease from 0.19 to below 0.01 out to a radius of 4 arcsec. Following Shields et al. (1990) estimate of the ratio of $\text{H}\alpha$ emission in the filament compared to the stellar cluster of region A, only

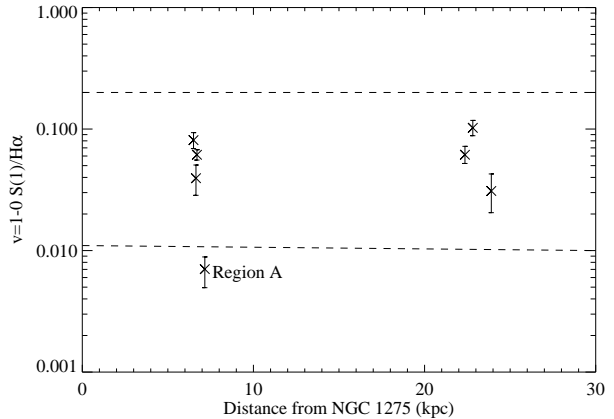


Figure 8. The line intensity ratio $v=1-0 \text{ S}(1)/\text{H}\alpha$ as a function of distance from the nucleus of NGC 1275. The region bounded by the dashed lines corresponds to the range of $v=1-0 \text{ S}(1)/\text{H}\alpha$ ratios in other nuclear regions of central cluster galaxies (Wilman et al. 2002). As there is no correlation with radius, the central AGN can not be exciting the molecular hydrogen

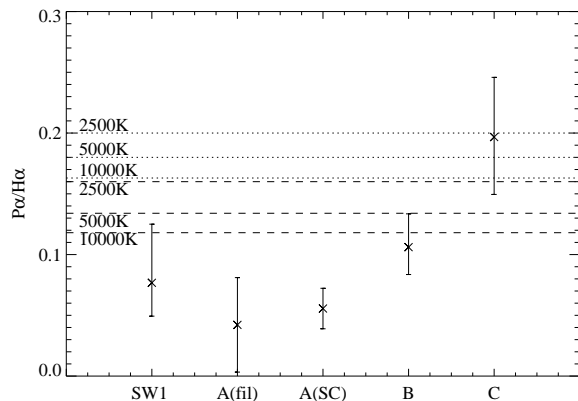


Figure 9. The line intensity ratio $\text{P}\alpha/\text{H}\alpha$ for regions in which $\text{P}\alpha$ could be measured or a reasonable estimate made. All errors follow from 1σ errors on the line intensities. The dotted lines give the expected ratio given Case A recombination with gas at the temperature written above the line. The dashed lines give the expected ratio given Case B recombination with gas at the temperature written below the line (Osterbrock 1989). $\text{P}\alpha$ emission from region A is divided into the broad and narrow component, with 30 per cent of the detected $\text{H}\alpha$ emission assumed to have come from the filamentary material, A(fil), and 70 per cent from the Stellar Cluster, A(SC).

30 per cent of the measured $\text{H}\alpha$ surface brightness has been taken into account for region A whereas all the $v=1-0 \text{ S}(1)$ emission has been taken into account. Even with this estimate, the ratio of region A falls below the other regions. Fig. 8 shows no correlation with distance from the central galaxy as would be expected if the active nucleus of NGC 1275 enhanced the HII or H_2 emission. We infer that the AGN can only play a minor role in exciting the filaments (Johnstone & Fabian 1988).

Possible excitation mechanisms that could produce these ratios have been discussed in a number of papers. Donahue et al. (2000) suggests X-ray heating of thick columns of molecular hydrogen, conduction from the ICM or mixing layers. These ratios could also be obtained from shocks according to the models

of Hollenbach & McKee (1989), whilst predictions of CLOUDY models, of dense self-gravitating clouds with $n_T = 10^5 \text{ cm}^{-3}$ exposed to UV radiation also produce these ratios (Wilman et al. 2002).

The $H\alpha$ intensity of the H_2 regions was estimated using aperture photometry on the Conselice et al. (2001) image (Fig 1) over the regions were the slits crossed. In doing so errors may be introduced by, for example, picking slightly different regions and different calibration methods. In addition no correction has been made to remove the [NII] line flux from the image or take into consideration any reddening which could have a large effect on this ratio. As it is difficult to assign an error to this, we can instead measure the $P\alpha/H\alpha$ ratios and compare them with predicted recombination ratios. Fig 9 shows the $P\alpha/H\alpha$ ratios for regions SW1, A, B and C together with various recombination ratios given by Osterbrock (1989). Although there is a large scatter, regions SW1, B and C all agree within error to Case B recombination ratios. The $P\alpha/H\alpha$ ratio for both the broad filamentary emission and the narrow stellar cluster emission of region A lies well below any expected recombination ratio. Therefore it is possible that the $v=1-0 S(1)/H\alpha$ ratio of region A is badly compromised by an inaccurate $H\alpha$ surface brightness estimate as well as an uncertain $v=1-0 S(1)$ line surface brightness.

4.4 Pressure Balance

The X-ray emitting gas surrounding the molecular hydrogen has a number density of $n \sim 0.06 \text{ cm}^{-3}$, and a temperature of approximately $3 \times 10^7 \text{ K}$, giving a thermal pressure of $\sim 1.8 \times 10^6 \text{ cm}^{-3} \text{ K}$ (Sanders et al. 2004). The pressure of the outer regions of the optical line-emitting gas has been estimated from the [SII] doublet (Heckman et al. 1989) and the gas is found to be approximately in pressure equilibrium with the surrounding X-ray medium. As the molecular hydrogen line ratios imply the emission is partially if not predominately thermal, with $T \sim 1600\text{-}2200 \text{ K}$, the total density from at least part of the molecular line-emitting region must be greater than the critical density above which thermal emission dominates, $n \geq 10^4 \text{ cm}^{-3}$. This implies the molecular line-emitting regions must be over-pressurized by at least 10 times that of its surrounding medium. This echoes the pressure problem raised by Wilman et al. (2002) and Jaffe et al. (2001) who postulated the need for a dynamic, non-isobaric model in order to explain both the ionized and molecular emission.

5 CONCLUSIONS

We have found molecular hydrogen emission from the same regions as the $H\alpha$ emission in the outer filaments, up to 24 kpc from the nucleus of the central cluster galaxy, NGC 1275. As H_2 quickly dissociates above temperatures of 4000 K, this finding proves that a cooler component is intimately associated with the extended optical/UV line-emitting filaments. The spectra are consistent with predominately thermal emission, whilst the ortho-to-para ratios of regions B and C suggest an additional non-thermal excitation component possibly from UV photons in the Lyman-Werner band. The high $H_2/Br\gamma$ ratios suggest that UV radiation from hot, young stars is unlikely, however there is $Ly\alpha$ emission and UV continuum associated with the optical filaments and X-ray irradiation of the molecular hydrogen by the surrounding ICM may be able generate enough photons in $Ly\alpha$ and in the Lyman-Werner

band through non-thermal electron collisions with hydrogen atoms (Maloney et al. 1996).

The measured excitation temperatures lie between 1600-2200 K and the column densities of the warm excited molecular hydrogen in these regions are $2\text{-}14 \times 10^{15} \text{ cm}^{-2}$. It is possible that there exists an even cooler component of molecular gas within these filaments which will be revealed only by searches for the $v = (0-0)$ pure rotational lines of hydrogen in the mid-IR, or CO emission in the mm waveband. As the emission is thermal, at least some of the emitting gas has a density greater than 10^4 cm^{-3} . Comparing the minimum pressure of the molecular line-emitting gas to that of the X-ray gas shows the molecular gas must be over-pressurized by at least an order of magnitude.

The presence of this molecular gas so far out in the ICM poses similar challenges as the presence of the optical line-emitting gas. Either the gas has formed in situ (having cooled from the ICM and is falling onto the galaxy in a condensing phase), or the gas has travelled from a much cooler region, abundant in molecular hydrogen, to where it has been detected in the ICM.

A large reservoir of molecular hydrogen is known to lie in the nucleus of NGC 1275 (Jaffe et al. 2001; Edge et al. 2002; Donahue et al. 2000; Krabbe et al. 2000). The origin of this gas is still debated, but it may have come from a previous merger as suggested by Braine et al. (1995) or be accumulated through cooling of the ICM. Theories have been proposed suggesting that the buoyant old radio bubbles, visible in X-ray images, drag gas from the central regions out into the ICM as they rise (Bohringer et al. 1995; Churazov et al. 2001; Fabian et al. 2003). In these models the filaments act as streamlines tracing the path of the cooler gas as it moves and is heated by the ICM.

The horseshoe-shaped filament and its mirror image seen to the West (see Fig. 1) in the NW, appears just below an old radio bubble with a flow pattern similar to that of water underneath a rising air bubble (see Fabian et al. 2003 for discussion). It is possible that the molecular hydrogen originated from the core of NGC 1275 and it is currently being heated as it is dragged into the hot ICM behind these buoyant bubbles. However not all optical emission-line filaments with molecular hydrogen appear to follow visible radio bubbles; in particular the radial filaments and molecular knots in the East do not point toward any known radio bubble. These filaments could have been drawn out by a bubble whose radio emission is now too faint to detect, although that would suggest that the molecular hydrogen exists in the hostile environment of the ICM for about $\sim 10^7\text{-}10^8$ years, thus having clear implications on the rate of conduction within the ICM. High velocity resolution spectroscopy of these filaments would enable mapping of any flow pattern and thus probe further the origin of this cool gas.

ACKNOWLEDGEMENTS

NAH and RMJ acknowledge support from PPARC and ACF and CSC thank the Royal Society for support. We thank the UKIRT support staff for all their help. The United Kingdom Infrared Telescope is operated by the Joint Astronomy Centre on behalf of the U.K. Particle Physics and Astronomy Research Council.

REFERENCES

- Allen S. W., Fabian A. C., Johnstone R. M., Arnaud K. A., Nulsen P. E. J., 2001, MNRAS, 322, 589

- Black J. H., van Dishoeck E. F., 1987, *ApJ*, 322, 412
- Bohringer H., Nulsen P. E. J., Braun R., Fabian A. C., 1995, *MNRAS*, 274, L67
- Braine J., Wyrowski F., Radford S. J. E., Henkel C., Lesch H., 1995, *A&A*, 293, 315
- Churazov E., Brüggem M., Kaiser C. R., Böhringer H., Forman W., 2001, *ApJ*, 554, 261
- Conselice C. J., Gallagher J. S., Wyse R. F. G., 2001, *AJ*, 122, 2281
- Crawford C. S., Allen S. W., Ebeling H., Edge A. C., Fabian A. C., 1999, *MNRAS*, 306, 857
- Donahue M., Mack J., Voit G. M., Sparks W., Elston R., Maloney P. R., 2000, *ApJ*, 545, 670
- Draine B. T., Bertoldi F., 1996, *ApJ*, 468, 269
- Draine B. T., Woods D. T., 1990, *ApJ*, 363, 464
- Edge A. C., 2001, *MNRAS*, 328, 762
- Edge A. C., Wilman R. J., Johnstone R. M., Crawford C. S., Fabian A. C., Allen S. W., 2002, *MNRAS*, 337, 49
- Fabian A. C., 2004, preprint, astro-ph/0407484
- Fabian A. C., Nulsen P. E. J., Arnaud K. A., 1984, *MNRAS*, 208, 179
- Fabian A. C., Sanders J. S., Crawford C. S., Conselice C. J., Gallagher J. S., Wyse R. F. G., 2003, *MNRAS*, 344, L48
- Heckman T. M., Baum S. A., van Breugel W. J. M., McCarthy P., 1989, *ApJ*, 338, 48
- Hollenbach D., McKee C. F., 1989, *ApJ*, 342, 306
- Jaffe W., Bremer M. N., 1997, *MNRAS*, 284, L1
- Jaffe W., Bremer M. N., van der Werf P. P., 2001, *MNRAS*, 324, 443
- Johnstone R. M., Fabian A. C., 1988, *MNRAS*, 233, 581
- Krabbe A., Sams B. J., Genzel R., Thatte N., Prada F., 2000, *A&A*, 354, 439
- Lepp S., McCray R., 1983, *ApJ*, 269, 560
- Lynds R., 1970, *ApJ*, 159, L151
- Maloney P. R., Hollenbach D. J., Tielens A. G. G. M., 1996, *ApJ*, 466, 561
- Mandy M. E., Martin P. G., 1993, *ApJS*, 86, 199
- Minkowski R., 1957, in *IAU Symp. 4: Radio astronomy*, p. 107
- Norgaard-Nielsen H. U., Hansen L., Jorgensen H. E., 1990, *A&A*, 240, 70
- Osterbrock D. E., 1989, *Astrophysics of Gaseous Nebulae and Active Galactic Nuclei*. University Science Books, p. 79
- Puxley P. J., Ramsay Howat S. K., Mountain C. M., 2000, *ApJ*, 529, 224
- Sabra B. M., Shields J. C., Filippenko A. V., 2000, *ApJ*, 545, 157
- Sanders J. S., Fabian A. C., Allen S. W., Schmidt R. W., 2004, *MNRAS*, 349, 952
- Schmidt R. W., Fabian A. C., Sanders J. S., 2002, *MNRAS*, 337, 71
- Shields J. C., Filippenko A. V., 1990, *ApJ*, 353, L7
- Shields J. C., Filippenko A. V., Basri G., 1990, *AJ*, 100, 1805
- Smith M. D., Davis C. J., Lioure A., 1997, *A&A*, 327, 1206
- Sternberg A., Dalgarno A., 1989, *ApJ*, 338, 197
- Sternberg A., Neufeld D. A., 1999, *ApJ*, 516, 371
- Tennant A. F., 1990, *NASA Technical Memorandum* 4301
- Turner J., Kirby-Docken K., Dalgarno A., 1977, *ApJS*, 35, 281
- Wilman R. J., Edge A. C., Johnstone R. M., Fabian A. C., Allen S. W., Crawford C. S., 2002, *MNRAS*, 337, 63